Secondary instabilities in the stabilized Kuramoto-Sivashinsky equation

Chaouqi Misbah* and Alexandre Valance†
Institut Laue-Langevin, Boîte Postale 156, 38042 Grenoble CEDEX 09, France
(Received 14 June 1993)

The Kuramoto-Sivashinsky (KS) equation is one of the simplest but generic nonlinear equations in dissipative systems, such as hydrodynamics and moving interfaces. The KS equation with a linear stabilizing term occurs in many situations: (i) directional solidification where kinetics are decisive and (ii) terrace-edge evolution in step-flow growth in the presence of step-step interaction. The first focus is to show the genericity of the KS equation. We then present an extensive analytical and numerical study of the stabilized KS equation. It is found that this equation reveals a variety of secondary bifurcations. Besides the usual Eckhaus instability, the cellular structure exhibits (i) a period-halving of the cellular state, (ii) parity breaking (PB), (iii) vacillating breathing (VB), and (iv) oscillation with a spatial wavelength "irrationally" related to the basic one. Among many other features, this equation manifests also a complex mixture of PB and VB, and pairs of anomalous cells, which are observed in many experimental situations. The occurrence of some of the secondary bifurcations (e.g., PB) is examined analytically in the vicinity of the codimension-2 bifurcation where the two modes q and $2q$ (q being the wave number) bifurcate, and for others (e.g., VB) by analogy with the problem of a quasifree electron in a crystal. Among other results reported here, we show that the VB mode is associated with the appearance of a wave-vector gap, due to a resonance between the "incident" wave and the "transmitted" one, while the analog of the Bragg resonance is not crucial. The analytical part of our investigation is supported by the full numerical calculation.

PACS number(s): 05.40.+j, 61.50.Cj, 68.55.−a

I. INTRODUCTION

One of the most common features in nonlinear dissipative systems is that they often spontaneously build up a spatially organized pattern from an initially structureless one when the system is brought away from equilibrium by varying a control parameter [1]. Well-known situations are encountered, for example, in hydrodynamics and crystal growth. A typical example in the first category is the Rayleigh-Bénard one: an initially quiescent fluid heated from below becomes unstable against the formation of rolls when the thermal gradient exceeds a certain critical value. Another well studied example is directional solidification; that is, pulling the sample at a constant speed in an external thermal gradient. It is well known that an initially planar solidification front becomes morphologically unstable when the pulling speed exceeds a certain critical value [2]; the front assumes a cellular periodic structure.

Near the instability threshold these systems can often, in principle, be described by simple models having a universal form, which go under the name of amplitude equations [3]. Further beyond the threshold, in the strongly nonlinear regime, it is sometimes possible to derive simple phase equations by perturbing about an ideal periodic structure [4]. The main outcome of such studies is the determination of the nature of the bifurcation (supercritical or subcritical) and the boundaries of the phase instability (the Eckhaus instability) in the parameter space. The Eckhaus instability is our first example of a secondary instability, in the sense that this instability corresponds to that of a cellular structure, which itself bifurcates from the initially structureless state (e.g., a quiescent fluid, a planar front). The instability of the structureless state is referred to as the primary instability.

More recent experimental efforts have led to the discovery of a myriad of other secondary instabilities. The most common one is the so-called broken-parity (BP) traveling state, the first pertinent experimental evidence of which is due to Simon, Bechoefer, and Libchaber [5] in the context of directional growth of a nematic phase. This state is characterized by the inclusion of a few asymmetric cells, escorted by two large domains of the *ordinary* symmetric state, which are approximately twice as large as the symmetric ones. As a consequence of parity breaking, the asymmetric domain travels sideways at a constant speed. Since that discovery, similar phenomena were found in eutectic systems [6], in the printer system [7], and in other various situations [8–11]. The fact that the asymmetric domains were first observed as small inclusions (a few cells) has led to their denomination: "solitary mode," "solitary waves," etc.

With regard to parity breaking, an important idea was put forward by Coullet, Goldstein, and Gunaratne [12], who suggested that the appearance of BP modes results from the loss of stability of the symmetric cells against parity-breaking fluctuations. They built a phenomenological picture that retained some interesting observed features. The suggestion of Coullet, Goldstein, and Gunaratne should imply that there exist extended BP

*Current address: Laboratoire de Spectrométrie Physique, Université Joseph Fourier, Grenoble I, B.P. 87, 38402 Saint-Martin-d'Héres Cedex, France.
†Also at Groupe de Physique des Solides, Universités Paris 7 et 6, 2 Place Jussieu, T. 23, 75005 Paris, France.

solutions (i.e., solutions that extend along the whole front, in the case of a moving interface) that travel sideways at a constant speed. Later, it was shown indeed, both for eutectics [13] and liquid-crystal systems [14,15], that such solutions exist; they emerge as a direct bifurcation from the initially symmetric pattern. An experimental suggestion [16] to have access to an extended BP state in the eutectic system—and thus to be in a situation similar to that dealt with in theoretical investigations—has been impressively demonstrated by Faivre and Mergy [17].

The second common example of secondary instabilities concerns the vacillating-breathing (VB) mode: each cell oscillates in phase opposition to its neighbors. This is a bifurcation that corresponds to a spatial period doubling and is oscillatory in time. This instability has been also observed in many systems [9]. By concentrating on the high-speed regime in the liquid-crystal systems we have shown recently [15] that the model equation does indeed support a VB solution, which results from the loss of stability of the symmetric pattern.

In a general framework, it is of great importance to know whether or not the number of possible secondary instabilities is finite, and if so how to classify them. Coullet and Iooss [18] use symmetry arguments to classify ten generic secondary instabilities; those presented above are typical examples. It is also crucial to know which of the potential instabilities are realized within a specific model. The studies mentioned above regarding PB and VB have proceeded along this line.

In general, dynamics involve complex equations, with sometimes nonlocal and retarded effects (the case of eutectics, for example), which make their complete description rather difficult. The large-speed regime reached by liquid-crystal experiments is theoretically a relatively tractable situation, where dynamics turn out to be quasi-local [19], (i.e., described by a nonlinear partial differential equation). Nevertheless, even in such a case dynamics still involve fancy nonlinearities and some aspect of retardation (propagative terms are present and not only diffusive). One of the challenges would be to recognize which of these nonlinearities are relevant and possibly to map them onto a picture exhibiting clearly their underlying physics. Also it is crucial to identify whether the propagative character of the equation is pertinent to the birth of some specific secondary instabilities, such as the VB one, or not. On the other hand, this kind of equation, although it describes remarkably well many interesting features for the specific liquid-crystal system, it does not possess any universality—at least without any renormalization procedure, which has not been attempted yet. It appears therefore strongly desirable to have at our disposal some generic model, for which to investigate the possible secondary bifurcations.

The purpose of this paper is to bring out, from a rather universal but relatively simple equation, a myriad of secondary instabilities. This is the stabilized Kuramoto-Sivashinsky (KS) [20,21] equation, which we shall write as

$$h_t = -\alpha h - h_{xx} - h_{xxxx} + h_x^2 , \tag{1.1}$$

where $h(x,t)$ is some dimensionless function (e.g., the front profile) of dimensionless space and time variables x and t, and α is a parameter that mimics a stabilizing effect (e.g., it is proportional to the thermal gradient in directional solidification or to the strength of step-step interaction in the step-flow growth; see next section). In this paper we shall first show that Eq. (1.1) is generic before proceeding to the search of its (rich) dynamics.

The usual KS equation (without the stabilizing term, $\alpha=0$) models a pattern formation in different contexts and is a paradigm of low-dimensional behavior in solutions to partial differential equations. Kuramoto [20] derived it in the context of reaction-diffusion equations modeling the Belousov-Zabotinskii reaction. Sivashinsky [21] derived it to model small thermal diffusive instabilities in laminar flame fronts. The equation arises also, among other situations, in Poiseuille flow of a film layer on an inclined plane [22], in solidification at large supercooling [23], and in the step-flow growth [24]. Numerous investigations were devoted to the KS equation, most of them focused, even with a (phenomenological) small stabilizing term, on the transition to chaotic solutions [25], which are exhibited by the KS equation at moderate aspect ratios. (The aspect ratio is defined here as the ratio of the size of the system to the typical stability length which corresponds to the neutral wavelength for infinitesimal perturbations about the solution $h=0$.)

The presence of the stabilizing term plays an important role (its physical origin for some systems will be described in the next section). It allows us to progressively increase the complexity of dynamics starting from the trivial solution ($h=0$). We shall see that this solution becomes unstable for a critical value of α and turns into a cellular structure, which in turn can lose its stability against various secondary instabilities. The surprising feature is that, despite its apparent simplicity (the only nonlinearity is quadratic), the stabilized KS equation manifests five generic instabilities, plus a rich set of tertiary instabilities. The five secondary instabilities are (i) the Eckhaus instability, (ii) the PB one, (iii) the period-halving one, where the cellular solution with the basic wave number q ceases to exist, (iv) the VB instability, and (v) an oscillatory instability with a spatial period "irrationally" related to the basic one. For brevity we use the abbreviation IVB (I stands for irrationality). It is fascinating that this simple equation manifests an even richer dynamics than apparently more complex equations [19,15]. In particular, the IVB mode has not been reported for any specific system, to our knowledge. This paper is a combination of an analytical and numerical efforts that allow us to shed light on various instabilities. Most of our reasoning will be easily exemplified by this simple equation, but we should keep in mind that it will work perfectly well with more complex equations.

In this paper we shall proceed along the following lines. In Sec. II we show in a general manner (without reference to any particular system) that the KS equation arises generically above bifurcations with a vanishing wave number; the vanishing character of the wave number is also generic and is traced back to symmetries. In the presence of an external field (e.g., a thermal gradient

in directional solidification) that breaks the symmetry under a translation $h \to h + c$, where c is a constant, we show that Eq. (1.1) is generic. Having motivated the genericity of the KS equation, we shall proceed to the search for secondary instabilities. The most well known of them is the Eckhaus instability, to which we devote a brief discussion in the Appendix. We first start in Sec. III with the determination of the steady-state periodic pattern, and specify the range of existence. The next step is devoted to the full stability problem by making use of the Floquet-Bloch theorem. We give the overall picture of our findings in Sec. IV. In Sec. V we shall be concerned with the dynamics close to the codimension-2 point where both the q and $2q$ (q is the wave number of the periodic structure) modes are dangerous. We reduce, in a coherent way, the original equation to a set of two complex amplitude equations for the two bifurcating modes. We show analytically that (i) the cellular mode undergoes a period-halving, where the steady-state solution with q as a basic wave number ceases to exist, whereby solutions with $2q$ as a basic wave number merge. This occurs when q is small enough (basically when the growth rates of both modes are of the same order). (ii) Before the period-halving bifurcation takes place, the mixed mode (where the q and $2q$ modes still coexist) undergoes a parity-breaking bifurcation. The full numerical calculation corroborates our analytical analysis. In Sec. VI, by analogy with the problem of a quasifree electron in a crystal, we develop a simple analytical treatment for the VB mode. We find that this mode, along with the one where the spatial periodicity is "irrationally" related to the basic one, results from a resonance between the "wave" function and its transmission. Our analysis captures the essential features of the full numerics. An analysis beyond secondary instabilities of the original equation will be given in Sec. VII, where we find, in particular, a mixture of VB and BP modes and the birth of pairs of anomalous cells (two asymmetric cells, with one being a mirror image of the other). Section VIII summarizes our results.

II. THE KS EQUATION AS A GENERIC EQUATION NEAR LONG-WAVELENGTH PRIMARY INSTABILITIES

In this section we show the generic character of the KS equation. Assume that the physical quantity of interest for a given system is described by a field $u(x,t)$. This quantity can be in the general case an N-dimensional vector, a function of the vector $\mathbf{x}$ in the d dimension and of time. Without loss of generality, we shall assume that the field is scalar, depending on a one-dimensional space variable x, and is a function of time. This means, in particular, that we consider the case of a purely codimension-1 primary bifurcation, so that the relaxing modes of the vector field can be adiabatically eliminated. As a consequence of this operation, the active field becomes scalar. For example, $u(x,t)$ can represent a one-dimensional instantaneous front position. In general, u obeys a nonlinear partial differential equation, or in some cases integrodifferential equations. We concentrate here only on the first category, and our reasoning will perfectly operate in the most general case. Therefore, u is taken to obey an equation of the form

$$L\left[\frac{\partial}{\partial t}, \frac{\partial^2}{\partial x^2}, \mu\right] u + N\left[\frac{\partial u}{\partial t}, \frac{\partial u}{\partial x}\right] = 0 , \tag{2.1}$$

where L and N stand for analytic linear and nonlinear differential operators, respectively, and μ mimics some control parameter. We require the parity symmetry with respect to x; that is, we assume that the original physical description of the system requires an equivalence between left and right. Note that this requirement is expressed explicitly on the linear operator.

In a completely translationally and rotationally invariant environment, it is clear that if u is a solution, then $u + \text{const}$ is also a solution. For example, if one fixes $z = u(x,t)$ to be the front position, then this position is determined only up to an additive constant, simply expressing the translational invariance along the z axis. If the front is moving in an external field (e.g., a liquid-solid interface moving in an external thermal gradient), however, then this invariance is broken.

Assume that the physical system described by the field u is susceptible to bifurcations. More precisely, assume that the trivial solution $u = 0$ becomes unstable for some critical value of the control parameter, say μ_c. The study of its stability is accomplished by looking for perturbations of the form

$$\delta u \sim e^{iqx + \omega t} + \text{c.c.} , \tag{2.2}$$

where q is the wave number and ω is the amplification (attenuation) rate. The solution $u = 0$ is unstable if $\mathrm{Re}(\omega) > 0$, at least for a particular q, while it is stable if $\mathrm{Re}(\omega) < 0$ for all q's. The critical situation (or bifurcation) is obtained when $\mathrm{Re}(\omega) = 0$ for a particular value of q, say $q = q_c$, and $\mathrm{Re}(\omega) < 0$ for all other values. This condition is expressed by

$$\omega = 0, \quad \frac{\partial \omega}{\partial q} = 0 . \tag{2.3}$$

Figure 1 shows schematically the situation (the bifurcation occurs for $\mu = \mu_c$). Note that we consider stationary primary bifurcations only.

An important point here is that, due to the rotational

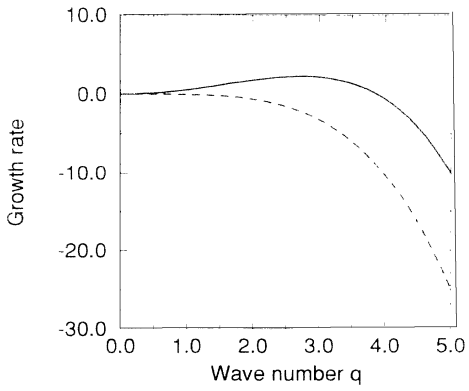

FIG. 1. Schematic plot of the dispersion relation. The dashed line represents the dispersion relation below the instability, while the full line, that above the instability. We anticipate here that the bifurcation occurs at $q = 0$ (see text below).

invariance, there always exists a neutral mode, $\omega=0$ for $q=0$. The invariance in the present case is that $u+\text{const}$ is also a solution of (2.1). This invariance has the important consequence that generically the bifurcation occurs at a vanishing wave number, $q_c=0$. Indeed, a bifurcation occurs only because two (or more) physical phenomena are competing. Since in the linear regime the two competing effects are superposable, we can assign to each effect its dispersion relation. Since the rotational symmetry holds for each of them, their growth rates vanish at $q=0$. Figure 2 shows schematically the behavior of both dispersion relations. We assume here that there exists a maximum wave number above which all perturbations decay. Physically this originates, for example, from surface tension for a front problem, or viscosity in hydrodynamics, and so on. On the other hand, each curve is, generically, tangent to the q axis at $q=0$ [because $\omega=\omega(q^2)$], and its curvature at that point is μ dependent. Two situations may happen: (i) the bifurcation occurs at $q=q_c\neq 0$, as shown in Fig. 3, which means that at small q the stabilizing effect is always dominant regardless of the value of μ, while at a particular value $q_c\neq 0$, the two competing effects counterbalance each other, and (ii) the bifurcation occurs at $q_c=0$, meaning that above a certain critical value of the control parameter μ_c the curvature of the growth rate of the destabilizing contribution exceeds that of the stabilizing one (Fig. 1). The second situation occurs generically, since the mode $q=0$ is always a dangerous mode, due to symmetry. We cannot, however, exclude the first type of bifurcation from (accidentally) occurring in principle (there is in fact no physical example known to us where the first type of bifurcation occurs). The aim of this section is to show that the dynamics above a bifurcation of type (ii) are described by a KS equation.

Let us now proceed to the calculation. In the linear regime we insert (2.2) into (2.1), and disregard the nonlinear part to obtain formally the dispersion relation

$$L(w,-q^2,\mu)=0 \ . \tag{2.4}$$

The linear stability analysis is the first natural step in any stability theory. Moreover, it allows one to determine the characteristic time and space scales close enough to the

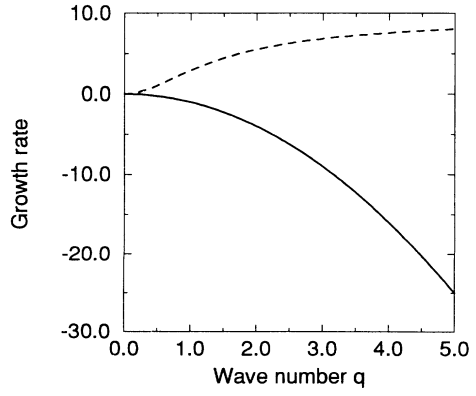

FIG. 2. Dashed line, the dispersion relation for the destabilizing effect; the full line, the dispersion relation for the stabilizing effect.

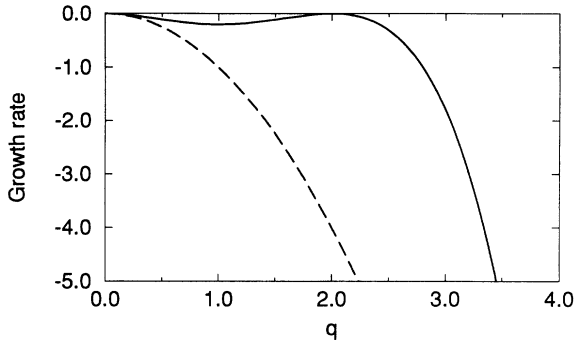

FIG. 3. Dispersion relation giving rise to a bifurcation at $q\neq 0$ (the full line); the dashed line represents the dispersion relation below the instability threshold.

bifurcation. Since close to the bifurcation $(\omega,q)\simeq(0,0)$, we expand (2.4) about this point

$$\omega L_1-q^2L_2+\frac{q^4}{2}L_{22}+\cdots=0 \ , \tag{2.5}$$

where L_1,L_2 represent the derivatives of L with respect to the first and second arguments, respectively. Note that all the constant terms should vanish because of the existence of a neutral mode at $q=0$. Before going further, an important remark should be made. In general the linear term in ω is present, and therefore we can neglect higher-order terms in ω, such as ω^2L_{11} and cross terms like ωq^2L_{12}. There is an example familiar to us, however, where the L_1 term vanishes close to bifurcation, and therefore there is a need to take these higher-order terms into account. The example in question is directional solidification [19] at high speed. In such a situation, it turns out that the governing equation is not of the KS type. If interface attachment kinetics are present, however, the L_1 term is present and KS dynamics [23] are recovered.

At the bifurcation, both relations (2.3) should hold. The first one is already exploited, while the second one yields at the bifurcation [by making use of (2.5); differentiation is made with respect to q^2]

$$L_2(0,0,\mu)=0 \ . \tag{2.6}$$

This means that there exists a critical value of μ, denoted by μ_c, at which the bifurcation occurs. Expanding L_2 about the bifurcation point, we obtain to leading order,

$$L_2=(\mu-\mu_c)L_{23}+(\text{higher-order terms}) \ . \tag{2.7}$$

Using this result we rewrite Eq. (2.5) to leading order as

$$L_1\omega=(\mu-\mu_c)L_{23}q^2-\frac{L_{22}}{2}q^4 \ . \tag{2.8}$$

Since we assume that (i) the trivial solution is unstable for $\mu>\mu_c$, and (ii) there exists a cutoff wave number above which all perturbations decay, L_{23}/L_1 and L_{22}/L_1 are both taken as positive. Figure 1 shows the growth rate ω below and above the instability. The quantity $\mu-\mu_c$ is the only small parameter that enters here. For brevity we introduce the notation

$$\epsilon=\mu-\mu_c \ . \tag{2.9}$$

From Eq. (2.8), we see that the wave number that corresponds to the maximum growth rate scales as $q_{\max} \sim \sqrt{\epsilon}$. This means that the wave packet that can be constructed with the active modes has a width of order $\sqrt{\epsilon}$ in Fourier space, or equivalently it varies on the scale of $1/\sqrt{\epsilon}$ in real space. We find it convenient to introduce a new variable,

$$X = \sqrt{\epsilon} x \ , \tag{2.10}$$

which offers the advantage that the small parameter will appear explicitly in the governing equation. In this variable the field u will vary on the scale of unity. Using the fact that the q's of interest scale as $\sqrt{\epsilon}$, we easily see from (2.8) that the growth rate scales as $\omega \sim \epsilon^2$. As for the spatial variation, we introduce a slow time variable T defined by

$$T = \epsilon^2 t \ . \tag{2.11}$$

Finally, because $u=0$ bifurcates to a nonzero value at $\mu=\mu_c$, we expect u to scale above and close to the instability as ϵ. We therefore write $u=\epsilon U$, where U is of order 1, and which we expand in a power series of ϵ,

$$u = \epsilon U(X,T) = \epsilon(U_0 + \epsilon U_1 + \cdots) \ . \tag{2.12}$$

Now the scheme is to use (2.10–2.12) together with (2.1) to deduce successively higher-order contributions in powers of ϵ.

Order ϵ. To this order we obtain

$$L(0,0,\mu_c)U_0 = 0 \ . \tag{2.13}$$

Since the factor L is equal to zero [expressing the condition $\omega(q=0)=0$; i.e., the existence of a translational mode], Eq. (2.13) is automatically satisfied, implying that U_0 is undetermined at this order. From now on all the arguments of the operators L and N are understood to be evaluated at the bifurcation.

Order ϵ^2. To this order we obtain

$$L_2 \frac{\partial^2 U_0}{\partial X^2} + L_3 U_0 = 0 \ , \tag{2.14}$$

$L_3=0$ (because of the existence of the translational mode) and $L_2=0$ (it expresses the second condition of the bifurcation $\partial\omega/\partial q=0$). That is to say the equation is also automatically satisfied at this order. The really interesting result emerges at the next order, where we obtain a constraint on U_0.

Order ϵ^3

After using the existence of a translational mode, together with the second bifurcation equation, we obtain

$$\frac{\partial U_0}{\partial T} + \frac{L_{23}}{L_1}\frac{\partial^2 U_0}{\partial X^2} + \frac{L_{22}}{2L_1}\frac{\partial^4 U_0}{\partial X^4} + \frac{N_2}{L_1}\left|\frac{\partial U_0}{\partial X}\right|^2 = 0 \ , \tag{2.15}$$

which is the KS equation, which we can rewrite in the following canonical form:

$$h_t = -h_{xx} - h_{xxxx} + h_x^2 \ , \tag{2.16}$$

after the following transformation

$$T = \frac{L_{22}L_1}{2L_{23}^2} t, \quad X = \left|\frac{L_{22}}{2L_{23}}\right|^{1/2} x, \quad U_0 = -\frac{L_{23}}{N_2} h \ . \tag{2.17}$$

The notations x and t here should not be confused with those used at the beginning of this section. Equation (2.16) constitutes a generic description close to criticality for a rotationally invariant system. This equation often appears in many contexts, but unfortunately in a somewhat disguised manner due, most of the time, to the fact that the explicit form of the equation is complex. A typical situation is encountered in crystal growth [23]. The present derivation shows clearly the generic origin of the KS equation. Note that the sign in front of the nonlinear term in Eq. (2.16) is unimportant, since it can be changed upon the transformation $h \to -h$ and without altering those of the other terms.

In the presence of an external field along the direction orthogonal to x, the translational invariance $u+\text{const}$ does not hold anymore. For example, a solidification front evolving into an external thermal gradient (directional solidification) has its mean position fixed by the thermal gradient at the melting temperature; the translational invariance (corresponding to a constant shift of the front position) is broken. This implies that the Goldstone mode is not a neutral mode. In our previous formulation, the expansion of the dispersion relation (2.4) contains an additional constant term

$$L_3 + \omega L_1 - q^2 L_2 + \frac{q^4}{2} L_{22} + \cdots = 0 \tag{2.18}$$

represented by L_3, and expressing the fact that for $q=0$, $\omega \neq 0$. We implicitly assume here that the bifurcation occurs at a small enough wave number, an assumption that implies that the term breaking the rotational invariance (the term L_3) should be weak enough. This is what we shall see below. The second bifurcation equation (2.3) provides exactly the same result as in the absence of an external field, since the derivative suppresses the constant term. In particular, we obtain that the bifurcation occurs at $q=0$. This means that at the bifurcation L_3 vanishes (this provides the bifurcation curve in the parameter space) and is small close to the bifurcation as we shall see below. We should mention that L_3 is a given physical field that is fixed from outside, and that therefore its value does not adjust to some specific value at the bifurcation. When we say that it vanishes at the bifurcation, this is taken to mean that the situation in the absence of this field is a reference one, and that we consider only weak deviations from this one. Stated in another way the effect of the external field will scale with some power of ϵ in such a way as to make the reasoning coherent. Slightly above the bifurcation, the wave number still scales as $\sqrt{\mu-\mu_c}$. The new feature now is that when we report this in the first bifurcation equation ($\omega=0$), which we have not yet exploited, we see from (2.18), after expansion about the critical point, that L_3 scales as $(\mu-\mu_c)^2$, as well as the growth rate. We can now repeat our ϵ expansion step by step. Since $L_3 \sim \epsilon^2$ and that $u \sim \epsilon$, the effect

of the external field shows up at third order in ϵ only. The result is

$$\frac{\tilde{L}_3}{L_1}U_0+\frac{\partial U_0}{\partial T}+\frac{L_{23}}{L_1}\frac{\partial^2 U_0}{\partial X^2}+\frac{L_{22}}{2L_1}\frac{\partial^4 U_0}{\partial X^4}+\frac{N_2}{L_1}\left[\frac{\partial U_0}{\partial X}\right]^2=0\ , \quad (2.19)$$

where we have set $L_3=\tilde{L}_3\epsilon^2$, with $\tilde{L}_3$ being of order unity. Introducing the same scales (2.17), we can rewrite (2.19) as

$$h_t=-\alpha h-h_{xx}-h_{xxxx}+h_x^2\ , \quad (2.20)$$

where

$$\alpha=\frac{\tilde{L}_3 L_{22}}{2L_{23}^2}\ . \quad (2.21)$$

Equation (2.20) is what we call the stabilized KS equation. Physically the stabilizing effect has different origins, depending on the physical system under consideration. For example, in directional solidification, the α term represents the effect of the applied thermal gradient [26]; in step-flow growth this role is played by step-step interaction [24]. Note that now there is no transformation to scale the parameter α out of the equation. This is the only parameter that enters our equation and that serves as a control parameter.

Now having show the generic character of the KS equation in the presence of damping, we shall deal with the general question of secondary instabilities. Before starting this program, some preliminaries are necessary.

III. STATIONARY PERIODIC SOLUTIONS

Let us first define the primary instability as the first stage for the formation of a cellular pattern. The dispersion relation for an infinitesimal perturbation about the solution $h=0(\delta h\sim e^{\omega t+ikx})$, which follows from Eq. (2.20), is given by

$$\omega=-\alpha+q^2-q^4\ . \quad (3.1)$$

The critical value of α, α_c, for the onset of the (primary) instability [see (2.3)] and the bifurcation wave number q_c are given by

$$\alpha_c=\frac{1}{4},\quad q_c=\frac{1}{\sqrt{2}}\ . \quad (3.2)$$

Figure 4 shows the neutral curve ($\omega=0$) in the α-q plane, below which the trivial solution is unstable. The maximum of the curve corresponds to the critical point given by Eq. (3.2).

The linear theory tells us that above the instability threshold the perturbations grow exponentially in the course of time, and therefore that the linear approximations should break down. In order to investigate the subsequent development of the instability, a nonlinear analysis must be performed. The nonlinear equations that arise in various situations, even as simple as Eq. (2.20) do not have analytical solutions, and in order to obtain precise information about the nonlinear regime, a resort to a numerical analysis is often unavoidable. Even in the situation where approached analytical results can be obtained, the numerical tool is a precious check of various approximations, and we shall meet this situation here. Close enough to the instability threshold a weakly nonlinear analysis is possible (see next section), but we first use "brute force" to give a complete picture of the stationary pattern by numerical solution. The steady-state version of Eq. (2.20) takes the form

$$-\alpha h_0-h_{0xx}-h_{0xxxx}+h_{0x}^2=0\ , \quad (3.3)$$

where $h_0(x)$ is the steady-state solution. Let us first consider periodic solutions with axial symmetry, and let q designate the basic wave number. We can thus restrict the domain of integration to a half period only, with the interval taken to be $[0,\lambda/2]$, where $\lambda=2\pi/q$. Equation (3.3) is of fourth order, thus requiring four conditions for the solution of the boundary-value problem. The symmetry condition imposes that $h_{0x}=0$ and $h_{0xxx}=0$ at the two ends of the integration interval, that is to say, we have four conditions. This means that a cellular steady-state solution exists, in principle, for arbitrary values of the wavelength. Figure 5 shows the domain of existence of the steady-state solution. Above a value $\alpha=0.15$ steady-state solutions exist every where inside the neutral curve. Below this value, there is a minimum wave number below which the solution with a basic wave number q ceases to exist: the q family runs into a *fold* singularity

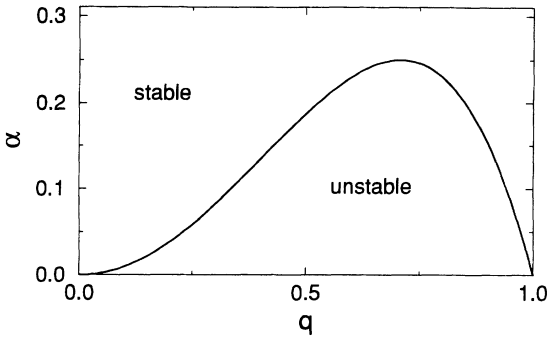

FIG. 4. Neutral curve separating a region where the trivial solution is stable from that where it is unstable.

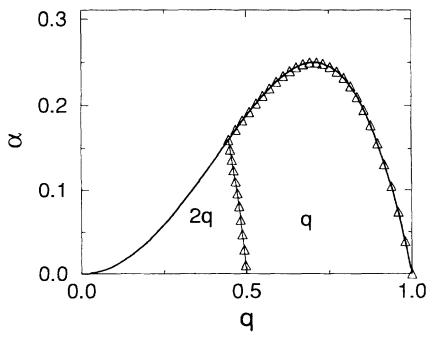

FIG. 5. Full line, the neutral curve. The symbols delimit the domain of existence of the steady-state solutions.

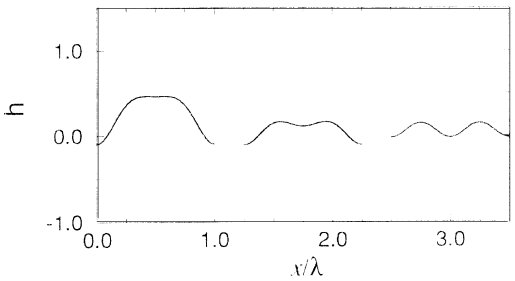

FIG. 6. Shape of the cellular solution for $\alpha=0.1$ and its evolution towards the *fold*. From right to left $q=0.47$, $q=0.48$, and $q=0.52$.

whereby solutions with $2q$ as basic wave number merge. This situation was met in many contexts [27,16]. Figure 6 shows the cellular solution and its evolution when q varies towards the *fold* singularity: the cellular solution first develops a negative curvature at the tip, before it halves its period at the *fold*. Note that the period-halving phenomenon occurs approximately for a wave number where the $2q$ mode becomes neutral, as can easily be checked in Fig. 6.

Having determined the region of existence of steady-state and periodic solutions, we are in a position to study their stability (secondary instabilities). The most known secondary instability is the Eckhaus one. This is a phase instability. The appearance of such an instability in a generic way when dealing with various systems can be traced back to a general symmetry: the translational symmetry along the x axis. Indeed, assume that $h_0(x)$ is a steady-state solution, then $h_0(x+\Phi)$ (where Φ is a constant phase shift) is also a solution. For an infinitesimal phase shift, we have $h_0(x+\Phi)=h_0(x)+\Phi\partial h_0/\partial x$. The quantity $\partial h_0/\partial x$ is nothing but the Goldstone mode, which is a neutral mode, and is conjugate to the phase shift of the pattern. The neutrality of such a mode simply expresses the fact that an extended system is indifferent to a global phase shift, due to translational invariance. A global phase shift then has an infinite relaxation time. In order to see whether such a mode might become unstable, we introduce a weak inhomogeneity in the phase and calculate the response function. The equation describing the phase evolution is of the diffusive type. For interested readers we present in the Appendix the extraction of the phase-diffusion equation in the context of the stabilized KS equation. This instability will also appear in another way when we use a systematic linear stability analysis of the periodic solution h_0.

IV. SECONDARY INSTABILITIES

In this section we deal with the full linear stability analysis of the cellular solution h_0. For that purpose we set $h(x,t)=h_0(x)+h_1(x,t)$ in Eq. (3.3) and neglect all but linear terms in h_1:

$$h_{1t}=-\alpha h_1-h_{1xx}-h_{1xxxx}+2h_{0x}h_{1x} . \tag{4.1}$$

This is a linear equation with periodic coefficient $[h_{0x}(x+\lambda)=h_{0x}]$. This entails that the linear operator commutes with the translational operator T_λ. This problem is similar to that of an electron in a crystal, and we shall return later to this analogy. Since Eq. (4.1) is autonomous with respect to time, the solution is proportional to $e^{\sigma t}$. The Floquet-Bloch theorem states that the general solution can be written as

$$h_1(x,t)=e^{\sigma_Q t+iQx}\hat{h}(x) , \tag{4.2}$$

where $\hat{h}$ has the same periodicity as the basic solution h_0, and Q is a real constant. Because of the periodicity of $\hat{h}$, it is sufficient to restrict Q to the first Brillouin zone, which we define as $Q\in[0,q]$. The next step is to expand both h_0 and $\hat{h}_1$ in Fourier series

$$h_0=\sum_{n=-\infty}^{\infty} A_n e^{inqx},\quad \hat{h}_1=\sum_{n=-\infty}^{\infty} c_n e^{inqx} . \tag{4.3}$$

Inserting this into Eq. (4.1) we obtain the equations for the coefficients c_n

$$\sigma_{Q,n}c_n=-[(nq+Q)^4-(nq+Q)^2+\alpha]c_n -2\sum_{m=-\infty}^{\infty}(mq+Q)(n-m)qA_{n-m}c_m . \tag{4.4}$$

This is an infinite set of equations that provides an infinite number of eigenvalues $\sigma_{Q,n}$ (the subscript n is to remind us that there are n eigenvalues for each Q) for each value of Q. In reality the number of active modes is limited, and one can legitimately truncate the matrix equation. For example, Fig. 7 shows that even for small values of α and q (say, 0.05 and 0.2) there are approximately only four modes that are unstable, while all the higher harmonics are damped and therefore slaved to the first four harmonics. For most of the calculation, including 20 modes has proven to be more than sufficient. Below we shall present all the instabilities we have found and give an overall picture.

A. The Eckhaus instability

This is the most generic instability, as discussed in the previous section. Slightly below the birth of the cellular solution (which appears at $\alpha_c=\frac{1}{4}$ and $q_c=1/\sqrt{2}$) we find

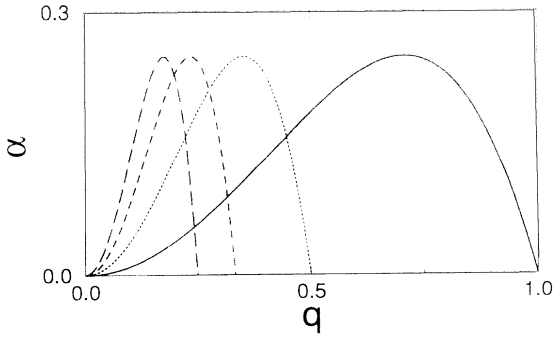

FIG. 7. Neutral curves for the first four harmonics. Long dashed line, $\omega(4q)=0$; dashed line, $\omega(3q)=0$; dotted line, $\omega(2q)=0$; and full line, $\omega(q)=0$. In the hatched region both the first and second harmonics are active, while the other ones are damped.

that the band of existence of these solutions is limited on both sides by a long-wavelength phase instability. More precisely, when q deviates from q_c towards large or small values, one finds that there is a critical q (for a given $\alpha < \alpha_c$) where the real part of one eigenvalue becomes positive (its imaginary part is zero), while all the others are negative. The analysis of the associated eigenmode shows that this corresponds to a phase mode. Figure 8 shows the eigenvalue below and above the instability threshold in the first Brillouin zone. As explained in the Appendix, the phase dynamics are described by a phase-diffusion equation of the form $\Phi_t = D\Phi_{xx}$, where D is the phase-diffusion coefficient. A phase instability is signaled by a negative phase-diffusion constant. Moreover, the dispersion relation following from the phase-diffusion equation is given by $\sigma = -DQ^2$. We have checked that $\sigma \sim Q^2$. In Fig. 9 the dashed lines represent the limit of the Eckhaus instability; the structure is unstable outside these boundaries.

The stability analysis gives information about the onset and the nature (by analyzing the eigenmodes) of the instability. In order to study the subsequent development of the instability, a full numerical solution of Eq. (2.20) is necessary. The principle of the numerical method is as follows. The spatial derivatives at each point of the discretization are evaluated by first calculating the Fourier transform of the interface, multiplying it with that power of the wave vector (times the imaginary unit) that corresponds to the order of the desired derivative, and transforming back to real space. The accuracy of this "infinite" order method compares impressively with a simple $O(h^2)$ (h being the mesh size) scheme in long-time runs. This gain in accuracy precludes, however, the investigation of large systems, because the matrix to be inverted in an implicit (time) integration scheme is not sparse. Once the derivatives are evaluated at all N points of the integration domain, we obtain formally N first-order differential equations. For the integration of this system we choose an implicit scheme that is appropriate for stiff differential equations in order to handle in particular dynamics close to bifurcations, and possibly to investigate the possibility of complex dynamics such as chaos. The adopted method is Gear's [28] backward difference method. Various checks have been made. In particular

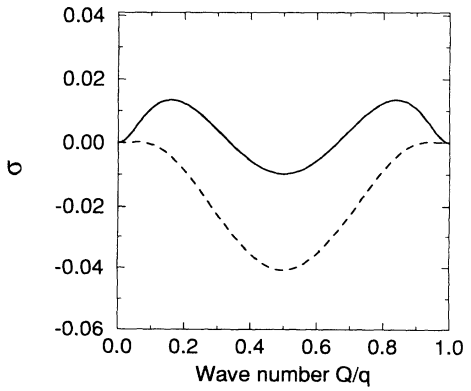

FIG. 8. Spectrum of the Eckhaus instability in the first Brillouin zone; below threshold (dashed) and above threshold (full).

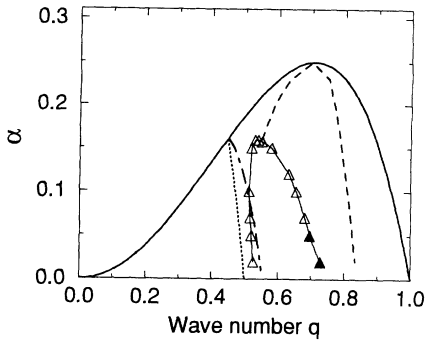

FIG. 9. Full phase diagram that results from the linear stability analysis. The dashed line, the boundary of the Eckhaus instability; the dotted line, the boundary below which the period-halving transition occurs; the dashed-dotted line, the boundary below which BP solutions appear; the empty symbols, the boundary of the VB mode; the filled symbols, the boundary of the IVB mode.

we have checked that the dynamical code reproduces well the steady-state solutions obtained by a shooting method.

Now we are in a position to show the full dynamical evolution of the Eckhaus instability. Since this is a long-wavelength instability, an integration with aspect ratios of the order of, or larger than, ten are necessary to allow the manifestation of the Eckhaus instability. Figure 10 shows the evolution of the solution. The initial wave number is taken inside the Eckhaus-unstable domain (right part in Fig. 9). One sees there that there is first a long-wavelength modulation of the phase, which eventually results in the destruction of cells (two cells in the present case). The wavelength adjustment occurs via a phase-diffusion process. The final wave number has decreased, and thus the structure reaches a wave number

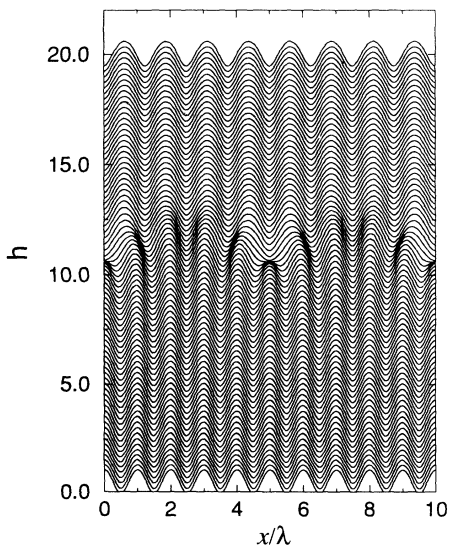

FIG. 10. Spatiotemporal portrait showing the dynamics of the Eckhaus instability. We start with $\alpha = 0.2$ and $q = 0.8$ (inside the Eckhaus unstable region). The final result is the destruction of two cells, and the final wave number is $q = 0.64$, which is inside the stable region.

inside the Eckhaus-stable region. Had we started with a wave number on the left part of the Eckhaus-unstable region, we would then have obtained the creation of new cells, thereby increasing the wave number.

B. The parity-breaking instability

Close to the primary instability, only the first harmonic is active, and the only instability is the Eckhaus one. As α decreases, the number of active modes increases. The second harmonic becomes competitive with the first one, and thus the dynamics are expected to become richer and richer. We have found that below $\alpha_1 \simeq 0.15$ (that is, when the second harmonic becomes dangerous) that (i) for large q's the Eckhaus instability still persists (note that in that region the second harmonic is damped), and (ii) in the small-q region a new instability appears in addition to the Eckhaus one. We represent the boundary below which the new instability appears by a dotted-dashed line in Fig. 9. This instability has the following feature: it appears in the center of the Brillouin zone ($Q=0$). That is to say, this is a homogeneous instability. The behavior of the spectrum below and above this instability is shown in Fig. 11. It is important to observe that the instability is present everywhere outside $Q=0$. This feature is found in another situation [29]. We believe that this feature is generic and is associated with the persistence of the Eckhaus instability. We shall see in Sec. VI that this results in the fact that the BP mode, although it can be observed as a localized mode (escaping thus the long-wavelength instability), will still potentially suffer long-wavelength instabilities. This explains why in most cases the BP mode manifests itself as a localized structure.

The eigenmode associated with this instability is antisymmetric, which breaks the symmetry $x \rightarrow -x$. Thus the appearance of this mode results from a parity-breaking instability inasmuch as the original equation of motion is symmetric under reflection at the symmetry axis. This instability has been observed experimentally in many systems and found theoretically in specific situations. The fact that the stabilized KS is one of the simplest nonlinear equations we can think of, and that its

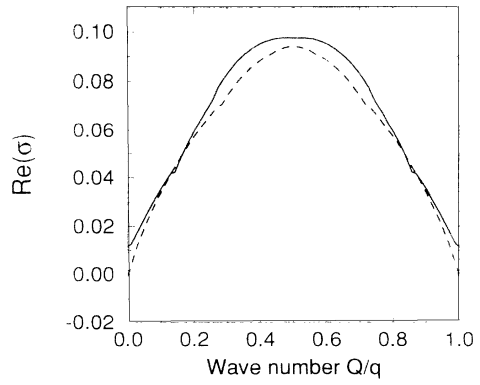

FIG. 11. Spectrum representing the PB instability. One sees that $\sigma(Q=0)\neq 0$. The dashed line, below the instability; the full line, above the instability.

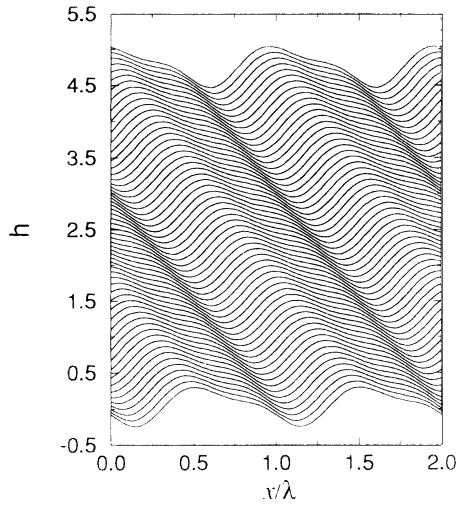

FIG. 12. Spatiotemporal portrait of the BP solution ($\alpha=0.15$, $q=0.46$).

form is generic points to the fact that parity breaking is a generic instability occurring at a sufficiently large wavelength.

Figure 12 shows the full dynamical solution after the parity-breaking bifurcation occurs. As a result of this symmetry breaking, the pattern drifts sideways. In the

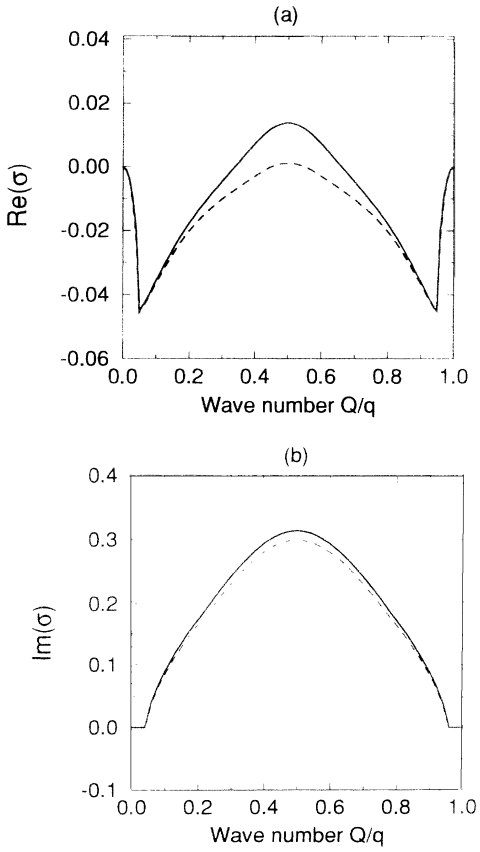

FIG. 13. Spectrum representing the VB instability. The dashed line, below the instability; the full line, above the instability. One sees that $\mathrm{Re}(\sigma)$ (a) crosses zero at $Q/q=\frac{1}{2}$, and $\mathrm{Im}(\sigma)\neq 0$ (b).

next section we shall deal with the analytical theory of secondary instabilities and shall see that the PB bifurcation occurs as a result of a resonant interaction of the first and second harmonics.

C. The vacillating-breathing mode

We have also identified another secondary instability that occurs in the middle of the first Brillouin zone (note that the two instabilities discussed above occurs at or close to $Q=0$) and is oscillatory in time. This is an oscillatory spatial-period-doubling instability that occurs below the boundary represented by empty triangles in Fig. 9. The associated spectrum is shown on Fig. 13, while Fig. 14 displays the dynamics of this mode. One sees there that each cell oscillates in phase opposition with its neighbors (vacillation), while the top of the cells vibrate in a breathing fashion. This mode has been observed on many systems and found numerically in the context of directional growth of a nematic phase [15]. The fact that here a very simple equation—but generic—reveals such a mode is also a signature of its genericity. In the next section we shall give our analytical understanding of such a mode based on an analogy with the problem of a quasifree electron in a crystal.

D. The "irrational" vacillating-breathing mode

The VB mode discussed in Sec. IV D results from an instability having a wavelength twice as large as the basic one—the critical wave number is at the middle of the Brillouin zone. As α decreases we find that the critical wave number deviates continuously from the center of the Brillouin zone; so to speak, it has no simple relation to the basic wave number. Having in mind the fact that the irrational numbers constitute a dense set of nonzero measure (in the jargon of number theory), we find it somewhat legitimate to call this mode *irrational vacillating-breathing mode*. Stated in another way, the new mode is generically incommensurate with the basic pattern. In Fig. 9 the filled triangles represent the boundary of the appearance of this mode, while its dynamics is shown in Fig. 15.

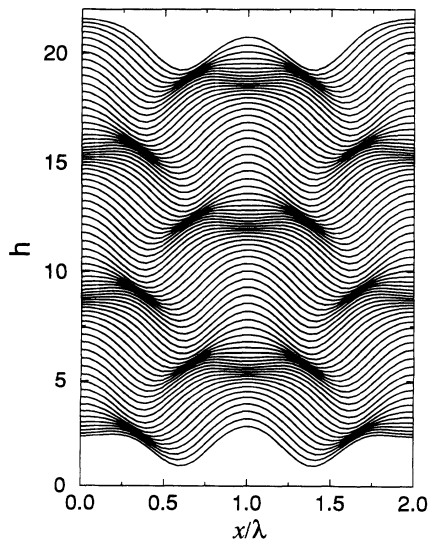

FIG. 14. Spatiotemporal portrait of the VB mode ($\alpha=0.1$, $q=0.64$).

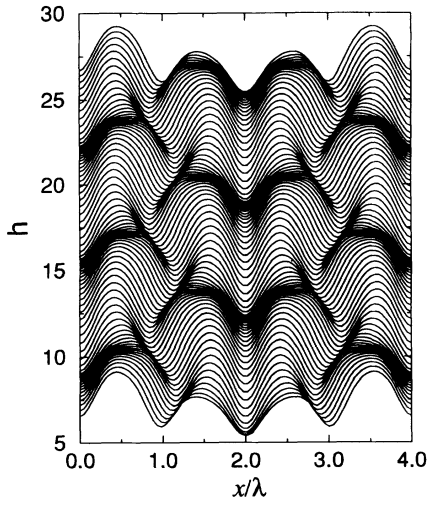

FIG. 15. Spatiotemporal portrait of the IVB mode ($\alpha=0.05$, $q=0.68$, $Q/q\simeq 0.3$).

E. The period-halving bifurcation

There exists another type of bifurcation, already discussed in Sec. III. When q decreases (at fixed $\alpha<0.15$), the cellular structure ceases to exist; the cells split altogether. The dotted line on Fig. 9 constitutes the boundary below which this occurs. In the next section we shall deal analytically with this bifurcation.

V. ANALYTICAL TREATMENT OF SECONDARY INSTABILITIES

Our aim here is to present our current analytical understanding of the secondary instabilities reported in the previous section. The Eckhaus instability, which is by now classical is discussed separately in the Appendix. The analytical examination of the parity-breaking instability is not a new description and is traced back to Malomed and Tribelsky [30]. The descriptions of the VB and IVB modes are novel aspects of the present paper. We feel it worthwhile to present also the analytic theory of the BP mode. Indeed, due to the simplicity of the KS equation, the analytical descriptions of various modes are easily exemplified in this equation, which serves as a pedagogical example for the understanding of secondary instabilities.

A central point for the description of the PB and the period-halving bifurcations is to map the full dynamics onto that of two resonant Fourier modes, while the VB and IVB necessitate another treatment. Let us first derive the equations for the two-mode coupling. An important point in the analysis is that we assume that only the first and second harmonics are active, while all higher harmonics are slaved to them. The corresponding region

in the parameter space is the dotted one in Fig. 7; on its right only the first harmonic is unstable. The first step is to expand $h(x,t)$ in Fourier series, $h=\sum_{n=-\infty}^{\infty}A_n(t)e^{iqx}$, and insert this into Eq. (2.20) to obtain

$$\dot{A}_n=\omega_n(q)A_n-\sum_{m=-\infty}^{\infty}(n-m)mq^2A_{n-m}A_m\ , \tag{5.1}$$

where we have set $\omega_n(q)=-(\alpha-n^2q^2+n^4q^4)$. We assume that the growth rates of the first and second harmonics are small enough for the truncation of the amplitude equations to make sense. This requirement is fulfilled if one concentrates on the situation close enough to the codimension-2 bifurcation (that is, close to the point where both harmonics are quasineutral). We shall also limit our expansion to third order in the amplitudes of the harmonics. Since in such a treatment the amplitude is proportional to the square root of the distance to the codimension-2 point (as is usually the case in a Landau expansion), higher-order terms induce negligibly small contributions. If we are interested in the dynamics of the first and second harmonics, one may be naively tempted to write (5.1) for $n=1$ and $n=2$, and keep in both equations only A_1 and A_2 up to third order in the amplitude expansion. This is however not quite legitimate. Indeed, although higher harmonics are damped they will still contribute to the dynamics of the first leading modes. To see this point it suffices to notice that in the equation of A_1 there are terms like $A_2^*A_3$ and that the slaving of the third harmonic to the first two induces $A_3\sim A_2A_1$ (note that both terms can be directly inferred from translational invariance), so that $A_2^*A_3\sim\|A_2\|^2A_1$, a term that should be retained. Similarly, in the equation for A_2 we must retain terms like $A_4A_2^*$, since from the slaving procedure $A_4\sim A_2^2$, so that $A_4A_2^*\sim\|A_2\|^2A_2$. Therefore to make a self-consistent calculation of the two-mode equations we must keep the leading terms containing A_3 and A_4, and express them as functions of the first two harmonics from the slaving conditions ($\dot{A}_3=\dot{A}_4=0$). Having taken care of this point, one can see that the calculation is then straightforward and leads to the two coupled equations

$$\dot{A}_1=\omega(q)A_1+4q^2A_1^*A_2+\frac{48q^2}{\omega(3q)}A_1\|A_2\|^2\ , \tag{5.2}$$

$$\dot{A}_2=\omega(2q)A_2-q^2A_1^2+\frac{24q^2}{\omega(3q)}A_2\|A_1\|^2+\frac{64q^2}{\omega(4q)}A_2\|A_2\|^2\ . \tag{5.3}$$

It is convenient to rewrite these equations by introducing the modulus and the phase of the complex amplitudes, $A_1=a_1e^{i\phi_1}$, $A_2=a_2e^{i\phi_2}$:

$$\dot{a}_1=\omega(q)a_1+4q^2a_1a_2\cos(\theta)+\frac{48q^2}{\omega(3q)}a_1a_2^2\ , \tag{5.4}$$

$$a_1\dot{\phi}_1=4q^2a_1a_2\sin(\theta)\ , \tag{5.5}$$

$$\dot{a}_2=\omega(2q)a_2-q^2a_1^2\cos(\theta)+\frac{24q^2}{\omega(3q)}a_2a_1^2+\frac{64q^2}{\omega(4q)}a_2^3\ , \tag{5.6}$$

$$a_2\dot{\phi}_2=q^2a_1^2\sin(\theta)\ , \tag{5.7}$$

where $\theta=\phi_2-2\phi_1$. From a simple algebraic manipulation of Eqs. (5.5) and (5.7) we obtain an equation for θ,

$$\dot{\theta}=q^2[a_1^2/a_2-8a_2]\sin(\theta)\ . \tag{5.8}$$

It is readily seen that the number of degrees of freedom is three; that is, Eqs. (5.4), (5.6), and (5.8) are closed equations for the three quantities (a_1,a_2,θ). Once the equations are solved for these quantities we can determine ϕ_1 and ϕ_2 from the detached equations (5.5), (5.7). This is a consequence of the translational invariance: one of the phases is arbitrary.

Since the field $h(x,t)$ in the two-mode interaction picture can be written as

$$\begin{aligned}h&=A_1e^{iqx}+A_2e^{2iqx}+\text{c.c.}\\&=2a_1\cos(qx+\phi_1)+2a_2\cos(\theta)\cos(2qx+2\phi_1)\\&\quad-2a_2\sin(\theta)\sin(2qx+2\phi_1)\ ,\end{aligned} \tag{5.9}$$

one sees that the profile contains an antisymmetric component as long as $\sin(\theta)$ is nonzero. Thus θ can be thought of as an orderlike parameter for the parity-breaking transition. Note also that as soon as $\theta=\text{const}\neq 0$, ϕ_1 (and ϕ_2) is a linear function of time [see Eq. (5.5)], stating that parity breaking induces a drift of the pattern. Below, we shall discuss the period-halving bifurcation and the parity-breaking one separately.

A. Period-halving bifurcation

Let us first concentrate on the situation where the pattern is symmetric. We then set $\theta=0$ or $\theta=\pi$ (and we shall see below that the two states are not identical; this is easily seen from (5.9) since in one case the second harmonic acts with a positive sign, while in the other case with a negative one).

1. Pure mode P^+ and P^-

Since we are interested in steady-state solutions, the equations of motion (5.4) and (5.6) take the form

$$\omega(q)\ a_1\mp 4q^2a_1a_2+\frac{48q^2}{\omega(3q)}a_1a_2^2=0\ , \tag{5.10}$$

$$\omega(2q)\ a_2\pm q^2a_1^2+\frac{24q^2}{\omega(3q)}a_2a_1^2+\frac{64q^2}{\omega(4q)}a_2^3=0\ , \tag{5.11}$$

where the upper (lower) sign corresponds to the P^+ (P^-) mode. Equation (5.10) has a trivial solution $a_1=0$, and it is the associated mode that we refer to as the *pure mode*. This is taken to mean that the contribution to the field is composed purely of the second harmonic only. It is easily seen that for this mode P^+ and P^- are identical and are characterized by

$$\begin{aligned}&a_1=0\ ,\\&\theta=\theta_+=\pi\quad(P_+)\ ,\\&\theta=\theta_-=0\quad(P_-)\ ,\\&a_2^2=-\frac{\omega(2q)\omega(4q)}{64q^2}>0\ .\end{aligned} \tag{5.12}$$

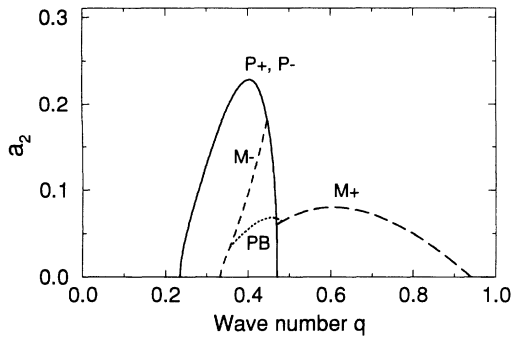

FIG. 16. Amplitude of second harmonic a_2 as a function of the wave number q in the two-mode interaction picture (see text).

Since the fourth harmonic is damped [$\omega(4q)<0$], the last condition is satisfied as long as $\omega(2q)>0$. In other words, the pure mode merges at the point where the second harmonic becomes neutral. Condition (5.12) is satisfied, for a given α, below a certain critical value of the wave number. The limit below which this occurs is shown by the dotted line in Fig. 9. We have also plotted in Fig. 16 the amplitude of the second harmonic as a function of q for $\alpha=0.1$.

2. *Mixed modes M^+ and M^-*

The mixed mode corresponds to the solution of (5.10) and (5.11), with $a_1\neq 0$. We can then solve for a_2 from Eq. (5.10) and report the result into (5.11) to solve for a_1. The result is

$$a_2=\frac{\omega(3q)}{48q^2}\left[\pm 2q^2-\left[4q^4-\frac{48q^2\omega(q)}{\omega(3q)}\right]^{1/2}\right], \tag{5.13}$$

$$a_1^2=\frac{a_2[\omega(2q)+64q^2a_2^2/\omega(4q)]}{\mp q^2-24q^2a_2/\omega(3q)}. \tag{5.14}$$

Since $\omega(3q)<0$ and $\omega(q)>0$, the argument of the square root is positive. So the only restriction for the existence of such a mode comes from the condition $a_1^2>0$. We should distinguish between the two types of modes. The result is

$$[\omega(2q)+64q^2a_2^2/\omega(4q)][q^2+24q^2a_2/\omega(3q)]<0 \quad (M_+), \tag{5.15}$$

$$\omega(2q)+64q^2a_2^2/\omega(4q)>0 \quad (M_-). \tag{5.16}$$

Since a_2 is given above by Eq. (5.13), the present condition corresponds to a region in the (α,q) plane. For a fixed $\alpha=0.1$, this branch is represented in Fig. 16.

One sees that if the equality in the above condition of existence holds simultaneously for both modes, we obtain $a_2^2=-\omega(2q)\omega(4q)/64q^2$, which is just the condition we obtained in the pure mode discussed above. That is to say, when this condition is met we have a transition from the mixed mode (where both the first and second harmonics are present) to the pure mode. Figure 16 shows the amplitude a_2 as a function of q for M^+ and M^-, where one observes that both branches branch off the pure mode one (but at different points).

B. Parity breaking

The question now is whether Eqs. (5.4), (5.6), and (5.8) can be solved for a nontrivial value of θ, and if so to determine the critical condition for the onset of bifurcation. Equation (5.8) can have a fixed point with a nontrivial value of θ. This happens if

$$a_1^2=8a_2^2. \tag{5.17}$$

The other conditions of stationarity of the pattern follow from the two remaining equations [Eqs. (5.4), (5.6)]:

$$\omega(q)\ a_1+4q^2a_1a_2\cos(\theta)+\frac{48q^2}{\omega(3q)}a_1a_2^2=0, \tag{5.18}$$

$$\omega(2q)\ a_2-q^2a_1^2\cos(\theta)+\frac{24q^2}{\omega(3q)}a_2a_1^2+\frac{64q^2}{\omega(4q)}a_2^3=0. \tag{5.19}$$

This set shows that a_1 and a_2 are both parametrized by θ, so that Eq. (5.17) is an implicit equation for θ. The procedure is easy in principle. It consists in using the condition (5.17) and solving for $\cos(\theta)$ and a_2^2 from Eqs. (5.18) and (5.19). We obtain

$$\cos(\theta)=-\frac{\omega(3q)\omega(q)+48q^2a_2^2}{4q^2\omega(3q)a_2}, \tag{5.20}$$

$$a_2^2=-\frac{[2\omega(q)+\omega(2q)]\omega(3q)\omega(4q)}{32[9\omega(4q)+2\omega(3q)]q^2}, \tag{5.21}$$

subject to the conditions [following from $a_2^2>0$ and $\|\cos(\theta)\|<1$]

$$\begin{aligned}&2\omega(q)+\omega(2q)>0,\\ &\|\omega(3q)\omega(q)+48q^2a_2^2\|<-4q^2\omega(3q)a_2,\end{aligned} \tag{5.22}$$

where we have taken into account the fact that $\omega(3q)$ and $\omega(4q)$ are both negative. These conditions define the domain of existence of the broken-parity state, where the "order parameter" θ is given by (5.20). Note that the first condition in (5.22) expresses the fact that at least one of the two modes should be active (i.e., having a positive growth rate) and that the damped one (if any) should not be highly damped. This explains that parity breaking occurs only if there is no dominance of one harmonic over the other, but only if both are competitive. In Fig. 16 we show the branch that corresponds to the broken-parity state, which bifurcates from the mixed M^+ mode slightly before the transition to the pure mode. It can easily be checked that the critical point where this happens corresponds to the loss of stability of the mode M^+ against homogeneous perturbations.

It is interesting to go back to Eq. (5.8) and expand it for small θ about the critical point defined above. It is a simple matter to show that, for a given α, the equation for θ takes, to leading order, the following form:

$$\dot{\theta}=(q^*-q)\beta\theta-\gamma\theta^3, \tag{5.23}$$

where β and γ are positive quantities (which can be expressed formally as functions of q and α), and q^* is the critical wave number below which nontrivial solutions exist. Equation (5.23) shows that parity breaking is a standard supercritical bifurcation.

Once we have found a fixed point corresponding to the BP mode we can return to Eqs. (5.5) and (5.7) to see the implication of the parity-breaking bifurcation. Since the BP mode corresponds to fixed points of (a_1,a_2,θ), the right-hand sides of (5.5) and (5.7) are independent of time, which implies that both phases are linear in time, so that Eq. (5.9) can be written as

$$h=2a_1\cos[q(x-vt)]+2a_2\cos(\theta)\cos[2q(x-vt)] -2a_2\sin(\theta)\sin[2q(x-vt)] , \quad (5.24)$$

where v, the drift velocity, is given by

$$v=-4qa_2\sin(\theta) . \quad (5.25)$$

One sees thus, as anticipated, that parity breaking results in a drift of the pattern. The field $h(x,t)=h(x-vt)$, and it is possible to go back to the original equation (2.20) and look for solutions of this form in the full analysis (beyond the two-mode coupling truncation). The result is a nonlinear eigenvalue problem for the unknown quantity v. We have solved this problem in order to compare our results with those obtained in the two-mode interaction picture. Suffice it here to say that as long as α is not too far from the codimension-2 point ($\alpha\sim 0.15$), the full calculation reproduces well the results summarized on Fig. 16.

C. The VB mode

In this section we present our understanding of the appearance of the VB mode. For that purpose we restart from Eq. (4.1)

$$\sigma h_1=-\alpha h_1-h_{1xx}-h_{1xxxx}+2h_{0x}h_{1x} , \quad (5.26)$$

where we have set $h_1(x,t)\sim e^{\sigma t}$. Equation (5.26) is reminiscent of the eigenvalue Schrödinger equation for an electron moving in a crystal, in the sense that it is a linear eigenvalue problem with spatially periodic coefficients. The analogue of the potential is $h_{0x}(x)$, which can be expanded in Fourier series, while the form of h_1 follows from the Floquet-Bloch theorem, as explained in Sec. IV. It can be written as

$$h_1=e^{iQx}[b_Q+b_{Q+q}e^{iqx}+b_{Q-q}e^{-iqx}+\cdots] , \quad (5.27)$$

where we have attributed to the amplitudes of the plane wave functions their total wave number as a subscript. The first term represents the "incident" wave function, while the second and third ones, the transmitted and reflected wave functions, respectively.

In the full numerics we found that at the critical point where the VB mode appears only the first harmonic in h_0 is important and that a_1 is as small as 0.25. Therefore the quantity $h_{0x}\sim qa_1=0.25$ ($q\sim 1$). As a consequence, and in a first step towards the understanding of the origin of the VB mode the "potential" h_{0x} in (5.26) can be treated in a perturbation theory (note that the other coefficients are of order unity). We are in a situation analogous to that encountered in the so-called quasi-free-electron limit. The eigenvalue $\sigma(Q)$ has the property $\sigma(Q+q)=\sigma(q)$, where q is the basic wave number. Let $\omega(Q)$ denote the eigenvalue of the bare problem, where Q belongs to the first Brillouin zone. This is given by $\omega(Q)=-\alpha+Q^2-Q^4$. This quantity is the analogue of the free-electron energy. It is convenient to represent this quantity in reciprocal space in the extended zone representation. Figure 17 shows this quantity. It is seen there, and because the topology of the present energy is more complicated than a parabola (because of the presence of a cut-off wave number), that we have three intersections close to the horizontal axis (and these are the most relevant since we are interested in those branches that potentially produce a neutral eigenvalue). The first intersection corresponds to the situation $\omega(Q)=\omega(Q-q)$, which leads to $Q=q/2$, and there is a second one that corresponds to $\omega(Q)=\omega(Q+q)$ and happens at Q not too far from $q/2$. The third intersection, unimportant here (as we shall discuss at the end of this section), corresponds to the intersection between the "$Q+q$" branch and "$Q-q$" one, and occurs at $Q=0$. The first case is similar to what happens in the quasi-free-electron problem, while the second one is a new aspect, and it is responsible for the appearance of the VB mode, as we shall see below. Let us consider each case separately.

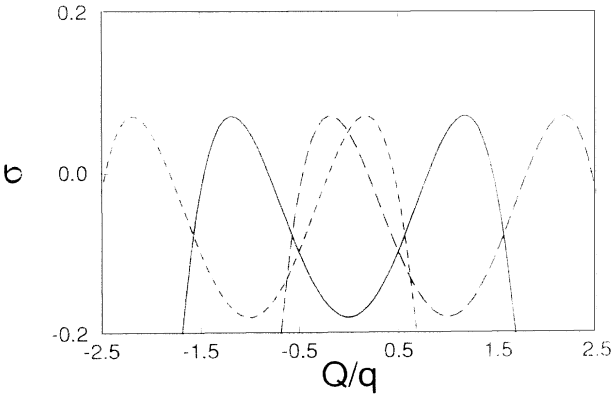

FIG. 17. Bare spectrum in the extended zone representation. One sees that there are two relevant intersections: one between the Q branch and the $Q-q$ one (which occurs at $Q/q=\frac{1}{2}$), and the other between Q branch and the $Q+q$ one, approximately at $Q/q\simeq 0.52$ (the third intersection is between the "$Q+q$" and "$Q+q$" branches, and is irrelevant for our purposes (see text).

1. *Resonance between the wave function and its reflection*

It is clear that the most important interaction of the nonperturbed states corresponds to the situation where the eigenvalues coincide. The first coincidence comes from the intersection of the bare spectrum of the incident wave function with that of the reflected one (the Bragg-like reflection), $\omega(Q)=\omega(Q-q)$. The eigenstate close to this intersection is a superposition of both wave functions

$$h_1 = b_Q e^{iQx} + b_{Q-q} e^{i(Q-q)x} . \tag{5.28}$$

Inserting this into (5.26), we obtain the following system:

$$\sigma b_{Q-q} = \omega(Q-q) b_{Q-q} + 2qQA_{-1} b_Q , \tag{5.29}$$

$$\sigma b_Q = \omega(Q) b_Q - 2q(Q-q) A_1 b_{Q-q} . \tag{5.30}$$

The associated eigenvalues are given by

$$\sigma = \tfrac{1}{2}\{\omega(q)+\omega(Q-q) \pm \sqrt{[\omega(q)-\omega(Q-q)]^2 - 16q^2Q(Q-q)\|A_1\|^2}\} . \tag{5.31}$$

Since $Q \le q$ (Q is confined to the first Brillouin zone), the argument of the square root is always positive, thus indicating that σ is real. At the intersection point, we have

$$\sigma = w(Q) \pm 2q^2 \|A_1\| . \tag{5.32}$$

This means that the resonant coupling between the wave function and its reflection results in the creation of a σ gap, similar to the energy gap in quantum mechanics. Figure 18(a) shows schematically the situation.

2. *Resonance between the wave function and its transmission*

In quantum mechanics there is only a creation of a σ gap. The reason is that the Hamiltonian is self-adjoint, implying that the eigenvalues are real. In the present problem the linear operator is not self-adjoint [due to the presence of h_{1x} in Eq. (5.26)]. Therefore complex eigenvalues are permissible. This will manifest itself by the appearance of a gap in Q axis, rather than in the σ one. This is what we shall obtain by analyzing the coupling between the wave function and its transmission. The associated mode takes the form

$$h_1 = b_Q e^{iQx} + b_{Q+q} e^{i(Q+q)x} , \tag{5.33}$$

which leads to the system

$$\sigma b_Q = \omega(Q) b_Q + 2q(Q-q) A_{-1} b_{Q+q} , \tag{5.34}$$

$$\sigma b_Q = \omega(Q+q) b_{Q+q} - 2qQA_1 b_Q , \tag{5.35}$$

resulting in the dispersion relation

$$\sigma = \tfrac{1}{2}\{\omega(q)+\omega(Q+q) \pm \sqrt{[\omega(q)-\omega(Q+q)]^2 - 16q^2Q(Q+q)\|A_1\|^2}\} . \tag{5.36}$$

At (and close to) the intersection point σ takes the form

$$\sigma = w(Q) \pm i2q\|A_1\|\sqrt{Q(q+Q)} . \tag{5.37}$$

One sees that now the resonance results in the appearance of a complex eigenvalue. We have checked that the frequency of oscillation is of the order of that obtained in the full linear stability analysis.

This is an unusual aspect that has no analogue in the problem of an electron in a crystal. Let us show that this result is equivalent to the appearance of a gap in the Q axis. For that purpose it suffices to expand (5.36) about the intersection point at fixed σ. The result is

$$\delta Q^2 = -\frac{4q^2Q(Q+q)\|A_1\|^2}{\omega'(Q)\omega'(Q+q)} , \tag{5.38}$$

where the prime designates differentiation with respect to Q, and δQ, the deviation from the intersection point. Since at the intersection of the Q and $Q+q$ branches, the slopes $\omega'(Q)$ and $\omega'(Q+q)$ have opposite signs, $\delta Q^2 > 0$: the resonance results indeed in the creation of a gap in the Q axis. Figure 18(b) shows schematically the result.

It is this mechanism from which originates the VB mode. To show it we have analyzed the full dispersion relation (5.36) in the parameter plane (α, q) and have investigated the spectrum as a function of Q. We have plotted in Fig. 19 the domain where both $\mathrm{Re}(\sigma) > 0$ and $\mathrm{Im}(\sigma) \neq 0$. The domain where $\mathrm{Re}(\sigma) > 0$ lies below the dashed line in Fig. 19, while that where $\mathrm{Im}(\sigma) \neq 0$, below the dashed-dotted line. In the domain below the intersection of these two curves we have both $\mathrm{Re}(\sigma) > 0$ and $\mathrm{Im}(\sigma) \neq 0$, which is the desired domain. The triangles represent the limit of the appearance of VB modes obtained in the full linear stability analysis presented in Sec. IV. As presented in that section, the VB mode survives down to $\alpha = 0.1$, while below this value the IVB mode prevails. That is to say, the most dangerous mode occurred first at $Q = q/2$, while by reducing α we found a

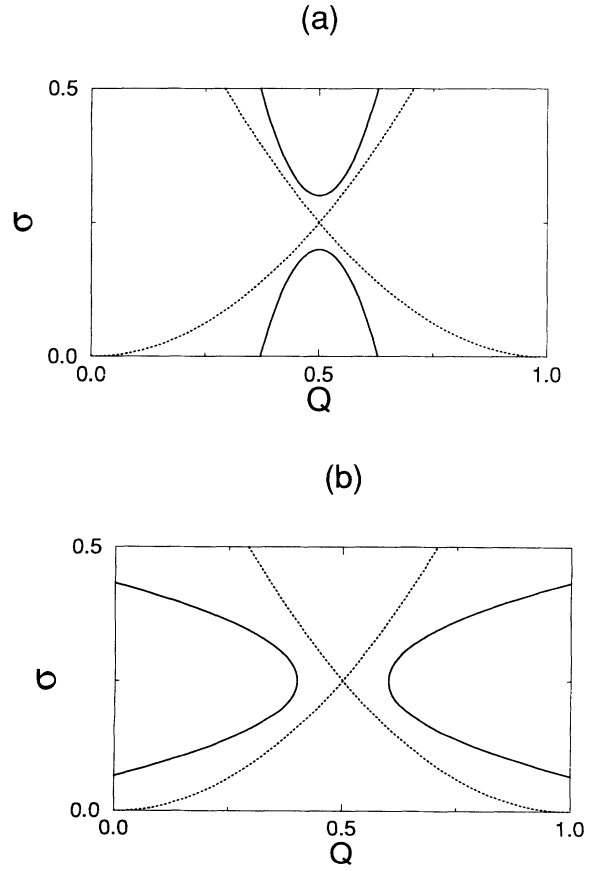

FIG. 18. Schematic plot showing the creation of a σ gap (a) and a Q gap (b).

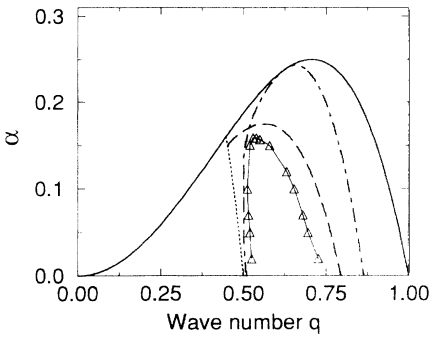

FIG. 19. Comparison between the analytical and the full calculation. Below the dashed-dotted line $\mathrm{Im}(\sigma)\neq 0$; below the dashed line $\mathrm{Re}(\sigma)>0$, the symbols are the results from the full calculation, and the dotted line delimits the period-halving boundary.

continuous deviation from this value. In our perturbation scheme, although we do not find a quite quantitative behavior, the same qualitative behavior is found. By including two higher-order reflections of the wave function we capture quantitatively the results of the full calculation. We should note that our perturbative calculation is valid (i) if the amplitude of the first harmonic is small enough, and (ii) if the other harmonics are negligible. By reducing the value of α both conditions become progressively violated. Indeed, the amplitude of the first harmonic becomes larger and larger as one moves away from the primary threshold, and the other harmonics become more and more active. It is for this reason that there is a discrepancy (as far as the pinning of Q at $q/2$) between the full calculation and the perturbative one when α is small enough. As our wish was to understand the basic ingredient of the appearance of the VB and IVB modes, we do not feel it worthwhile to linger here on details.

Two remarks are in order. First, our analysis is pedestrian and captures the essential features. Second, although our reasoning was put into practice on the stabilized KS equation, the present analysis can be used in more complex situations. In particular, we have drawn similar conclusions from more complicated equations [29].

Finally, it can easily be recognized that the "$Q+q$" and "$Q-q$" waves do not couple to leading order in the amplitude expansion of h_0. More precisely, their coupling is mediated by the second harmonic (with A_2 as an amplitude). It is a simple matter to include the second harmonic to treat this coupling. Emerging from this analysis is the creation of a σ gap.

VI. BEYOND SECONDARY INSTABILITIES

Hitherto, we were concerned with the birth of secondary modes and their subsequent dynamics for small aspect ratios (except the Eckhaus instability) and in a limited range of parameters. The question naturally arises of whether or not the secondary modes are everywhere stable. For example, would these modes survive for larger aspect ratios? Since the Goldstone mode is still present due to translational invariance, it is legitimate to expect that some of the modes may suffer long-wavelength instabilities, and this is what happens to the BP mode, for example. We did not make an exhaustive study of the dynamics. We have nevertheless important information, for which we give only a brief account. We discuss separately various results.

A. Mixture of VB and BP modes

We have investigated the evolution of the VB mode. In Sec. IV we have already shown the dynamics (Fig. 14) at $\alpha=0.1$ and $q\sim 0.64$, which is not far from its birth. As α decreases the limit cycle associated with the VB mode undergoes an instability that is parity breaking. The pattern drifts sideways while the VB mode subsists. The behavior is shown in Fig. 20. It is important to know whether each mode maintains its identity or not, or in other words whether the ratio of the two temporal frequencies associated with both modes is rational or irrational. To answer this question we have computed the Poincaré map. For the parameter values we have investigated so far, we have only found either a mode locking or a weak incommensurability of the two modes. In the first case this means that the Poincaré map consists of isolated spots, while in the second case this means that the Poincaré map is not covered densely (or that the trajectories do not cover the torus in phase space densely). At present this also indicates most likely that this mode is not a prelude to temporal chaos, contrary to what was found in another situation [15].

B. Long-wavelength instabilities of the BP mode

This question was motivated by a result obtained by Fauve, Douady, and Thual [31] on the normal form of Coullet *et al.* [12]. Indeed Coullet, Goldstein, and Gunaratne [12] have written a coupled amplitude-phase equation for the parity-breaking mode, inferred from symmetry arguments. Fauve, Douady, and Thual [31] have pointed out that the homogeneous BP state suffers a

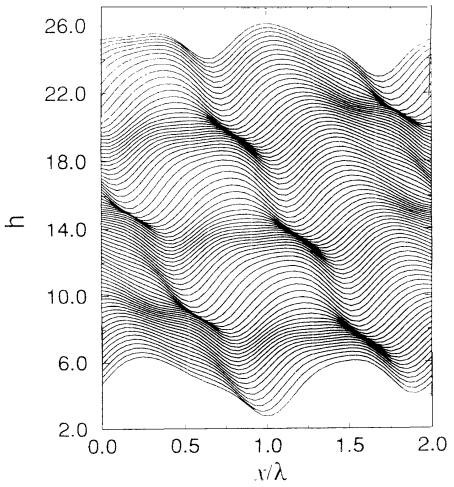

FIG. 20. Spatiotemporal portrait showing a mixture of a VB and a BP mode ($\alpha=0.048$, $q=0.53$).

long-wavelength oscillatory instability close enough to the critical point. We investigated this question both by performing the full linear stability analysis of the BP state and by solving numerically the time-dependent nonlinear equation. The linear stability analysis shows indeed that the BP mode suffers a long-wavelength oscillatory instability close enough to the critical point, as found from the equation of Coullet, Goldstein, and Gunaratne [12]. The full dynamics, which is still in progress, shows that an initial extended BP state is indeed unstable: the state exhibits fragmentations initiated by the creation or destruction of cells, leading ultimately to a modulated structure. This (long-wavelength) instability is most likely the reason why one often sees in experiments only localized asymmetric cells. We hope to pursue our analysis, in particular to answer the important question of wavelength selection mediated by the persistent passage of the "solitary" asymmetric wave, as expected from the analysis of Coullet, Goldstein, and Gunaratne [12], who assume a subcritical parity-breaking bifurcation, and that of Caroli, Caroli, and Fauve [32], who dealt with a supercritical bifurcation, as encountered here.

C. Anomalous cells

There are many experimental situations where the pattern exhibits a pair of so-called *anomalous cells.* This is a pair of two neighboring cells, each asymmetric and a mirror image of the other. Our belief is that the origin of this cell doublet is the same as that of parity breaking. Because parity breaking is a pitchfork bifurcation, there is a degeneracy lying in the fact that right- and left-traveling states are physically equivalent. Thus, we can imagine that each cell may maintain its identity, and choose the right one, while the neighbor, the left one. This feature is somewhat similar to that encountered in ferromagnet domain structures.

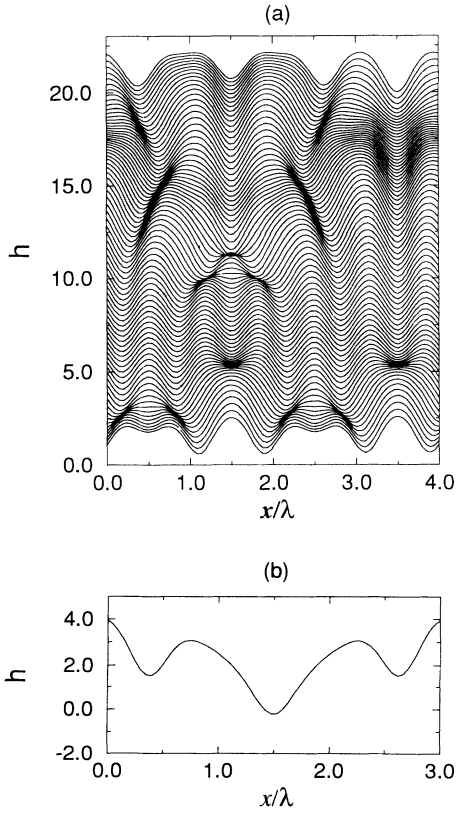

FIG. 21. Dynamics showing the creation of pairs of anomalous cells and their destruction and so on (a). In (b) we have plotted the anomalous cells.

In a stationary regime, we have not yet investigated this question, and hope to elucidate it in the future. We have found, however, in the numerical study of the full equation, for moderate aspect ratio (about four), the appearance of anomalous cells. This structure did not manifest itself here as a permanent one, at least for the range of parameters explored so far. The anomalous doublet occurs from the VB mode; it nucleates after a cell creation (Fig. 21), and then the doublet disappears, and so on. Our study is very preliminary, but clearly shows the presence of an underlying fixed point of an extended anomalous state.

VII. CONCLUSION

We have presented an extensive study on secondary instabilities, plus some preliminary results that go beyond this. Our analysis is a combination of analytical and numerical work. We have given a proof of the genericity of the equation for which this study has been done. We expect therefore the results presented here to concern generically nonequilibrium pattern-forming systems. There is indeed an increasing number of physical systems that manifest features found in the present study. There is, to our knowledge, yet no experimental evidence, however, for the IVB mode. It was fascinating to see that despite the simplicity of the stabilized KS equation (one of the simplest nonlinear equation we can imagine) it exhibits a rich variety of steady and dynamical features.

Although this work has dealt with a number of features, it is far from having exhausted all possible dynamics. For example, the question of the "solitary" dynamics, and its implication on wavelength selection is of paramount importance to guide future work on this long-standing puzzle, and the stabilized KS equation is an appropriate candidate for the study of this question.

Finally, little is known about interface dynamics for a true two-dimensional front. There we expect many new features that have no topological analogue in the one-dimensional front, such as chirality. The generalization of the stabilized KS equation to this situation is straightforward, and it is clear now that the advantage in using the stabilized KS equation in such a context is obvious.

ACKNOWLEDGMENTS

We are grateful to the Centre Grenoblois de Calcul Vectoriel for providing us with computing facilities.

APPENDIX: THE PHASE-DIFFUSION EQUATION

In this appendix we extract from Eq. (2.20) the part that is relevant to phase dynamics. For that purpose we use a similar method to that used in other contexts [4].

As stated before, the Goldstone mode is neutral, meaning that a constant phase shift has an infinite relaxation time, due to translational invariance. In order to see whether this mode is dangerous, and if so under which condition, we introduce a small inhomogeneity in the phase. That is to say we look for long-wavelength perturbations of the phase of the pattern. For a completely homogeneous pattern, the field is 2π periodic in the phase ϕ. In the presence of inhomogeneity, the phase ϕ is a function of space and possibly time, $\phi(x,t)$. Accordingly, the local wave number $q(x,t)=\partial\phi/\partial x$ varies in space and time. The demand that the wave number be a slow function of x is satisfied by requiring that the phase ϕ scales as $\phi\sim\Phi(X,t)/\epsilon$, where Φ is a slow function of space, as explicitly shown by the introduction of a slow variable $X=\epsilon x$, where ϵ is an auxiliary small parameter measuring the strength of the phase modulation. On the other hand, due to the Onsager law, we expect any inhomogeneity to result in a phase-diffusion current. Therefore we expect the time scale of the motion of interest to be of order ϵ^2. Accordingly, we introduce a slow variable $\tau=\epsilon^2 t$, so that the fast phase scales as

$$\phi=\frac{\Phi(X,\tau)}{\epsilon} \ . \tag{A1}$$

The introduction of slow scales means that we consider formally h as a function of the three (independent) variables (ϕ,X,τ). We are therefore to understand that we must make the substitutions (to leading order in ϵ)

$$\frac{\partial}{\partial x}\to q\frac{\partial}{\partial\phi}+\epsilon\frac{\partial}{\partial X}, \quad \frac{\partial}{\partial t}\to\frac{\partial\Phi}{\partial\tau}\frac{\partial}{\partial\phi} \ . \tag{A2}$$

The pattern responds to the phase modulation, so that h is written as

$$h(\phi,X,\tau)=h_0+\epsilon h_1+\cdots \ . \tag{A3}$$

The strategy now is to insert (A2) together with (A3) into the governing Eq. (2.20) and deduce successively higher-order contributions in powers of ϵ.

Order ϵ^0. To this order we obtain

$$-\alpha h_0-q^2h_{0\phi\phi}-q^4h_{0\phi\phi\phi\phi}+q^2h_{0\phi}^2=0 \ . \tag{A4}$$

This is the steady-state version of (2.20) parametrized by the local wave number q.

Order ϵ^1. To this order we obtain

$$-\alpha h_1-q^2h_{1\phi\phi}-q^4h_{1\phi\phi\phi\phi}+2q^2h_{0\phi}h_{1\phi}=F(\phi,X,\tau) \ , \tag{A5}$$

where

$$\begin{aligned}F=&\Phi_\tau h_{0\phi}-2qh_{0\phi}h_{0X}+qh_{0\phi X}+(qh_{0\phi})_X\\&+q^3h_{0X\phi\phi\phi}+q^2(qh_{0\phi\phi\phi})_X\\&+q(q^2h_{0\phi\phi\phi})_X+(q^3h_{0\phi\phi\phi})_X \ .\end{aligned} \tag{A6}$$

It is easy to recognize that the linear operator on the left-hand side of (A5) admits the translational mode $(h_{0\phi})$ as a null eigenmode [it suffices to differentiate (A4) to see this result]. The Freedholm alternative theorem then states that this problem is solvable only if the right-handside of Eq. (A5) is orthogonal to the null space of the adjoint operator. Let us establish this result directly. Let $h_1^\dagger$ designate the adjoint function to h_1, which we take to be 2π periodic in ϕ. Multiply Eq. (A5) by $h_1^\dagger$ and integrate over ϕ from 0 to 2π. The second and fourth derivatives in Eq. (A5) are obviously self-adjoint, while this is not the case with the first derivative. After integration by parts (the boundary terms vanish due to periodicity), we obtain

$$\int_0^{2\pi}d\phi\, h_1L^\dagger h_1^\dagger=\int_0^{2\pi}d\phi\, h_1^\dagger F(\phi,X,\tau) \ , \tag{A7}$$

where $L^\dagger$ is the adjoint operator defined by

$$L^\dagger h_1^\dagger=-\alpha h_1^\dagger-q^2h_{1\phi\phi}^\dagger-q^4h_{1\phi\phi\phi\phi}^\dagger-2q^2(h_{0\phi}h_{1\phi}^\dagger)_\phi \ . \tag{A8}$$

Since $h_1^\dagger$ belongs to the kernel of $L^\dagger$, we obtain from (A7) the phase-diffusion equation

$$\Phi_\tau=D\Phi_{XX} \ , \tag{A9}$$

where the phase-diffusion coefficient D is given by

$$D=\left|\int_0^{2\pi}d\phi\, h_1^\dagger\left|-2qh_{0\phi}h_{0q}+qh_{0\phi q}+(qh_{0\phi})_q+q^3h_{0q\phi\phi\phi}+q^2(qh_{0\phi\phi\phi})_q+q(q^2h_{0\phi\phi\phi})_q+(q^3h_{0\phi\phi\phi})_q\right|\right|\Big/\int_0^{2\pi}d\phi\, h_{0\phi}h_1^\dagger \ . \tag{A10}$$

A phase instability is signaled by a negative diffusion constant. The computation of the phase-diffusion coefficient requires the determination of both the steady-state solution and the adjoint function. The first question has already been discussed in Sec. III. The adjoint function obeys a linear homogeneous equation, $L^\dagger h_1^\dagger=0$, which can be solved by means of a singular value decomposition method, used in another context [4,19]. The results obtained from phase dynamics agree with those following from the full linear stability analysis.

[1] M. C. Cross and P. C. Hohenberg, Rev. Mod. Phys. (to be published).
[2] W. W. Mullins and R. F. Sekerka, J. Appl. Phys. **35**, 444 (1964).
[3] A. C. Newell and J. C. Whitehead, J. Fluid Mech. **38**, 279 (1969); L. A. Segel, *ibid.* **38**, 203 (1969).
[4] K. Brattkus and C. Misbah, Phys. Rev. Lett. **64**, 1935 (1990), and references therein.

[5] A. J. Simon, J. Bechhoefer, and A. Libchaber, Phys. Rev. Lett. **63**, 2574 (1988).
[6] C. Faivre, S. de Cheveigné, C. Guthmann, and P. Kurowski, Europhys. Lett. **9**, 779 (1989).
[7] M. Rabaud, S. Michalland, and Y. Couder, Phys. Rev. Lett. **64**, 184 (1990).
[8] P. Oswald, J. Phys. (France) II **1**, 571 (1991).
[9] For a recent review see J. M. Flesselles, A. J. Simon, and A. J. Libchaber, Adv. Phys. **40**, 1 (1991).
[10] I. Matabazi, H. Hegset, C. D. Andereck, and J. Wesfreid, Phys. Rev. Lett. **64**, 1729 (1990).
[11] L. Limat, P. Jenffer, B. Dagens, E. Touron, M. Fermigier, and J. E. Wesfreid, Physica D **61**, 166 (1992).
[12] P. Coullet, R. Goldstein, and G. H. Gunaratne, Phys. Rev. Lett. **63**, 2574 (1989).
[13] K. Kassner and C. Misbah, Phys. Rev. Lett. **65**, 1458 (1990); **66**, 522(E) (1991); C. Misbah and D. E. Temekin, Phys. Rev. A **46**, R4497 (1992).
[14] H. Levine and W. J. Rappel, Phys. Rev. A **42**, 7475 (1990).
[15] K. Kassner, C. Misbah, and H. Müller-Krumbhaar, Phys. Rev. Lett. **67**, 1551 (1991); A. Balance, Stage de DEA, Université de Paris 7, 1991.
[16] K. Kassner and C. Misbah, Phys. Rev. A **44**, 6533 (1991).
[17] G. Faivre and J. Mergy, Phys. Rev. A **45**, 7320 (1992).
[18] P. Coullet and G. Iooss, Phys. Rev. Lett. **64**, 866 (1990).
[19] A. Ghazali and C. Misbah, Phys. Rev. A **46**, 5026 (1992).
[20] Y. Kuramoto and T. Tsuzuki, Prog. Theor. Phys. **55**, 356 (1976).
[21] G. I. Sivashinsky, Acta Astraunautica **4**, 1177 (1977).
[22] D. J. Benney, J. Math. Phys. (N.Y.) **45**, 150 (1966).
[23] C. Misbah, H. Müller-Krumbhaar, and D. E. Temkin, J. Phys. (France) I **1**, 585 (1991).
[24] I. Bena, C. Misbah, and A. Valance, Phys. Rev. B **47**, 7408 (1993).
[25] P. Manneville, in *Propagation in Systems Far From Equilibrium,* edited by J. E. Wesfreid, H. R. Brand, P. Manneville, G. Albinet, and N. Boccara (Springer-Verlag, Berlin, 1988).
[26] A. Novick-Cohen, Physica **26D**, 403 (1987).
[27] L. H. Ungar and R. A. Brown, Phys. Rev. B **29**, 1367 (1984).
[28] C. W. Gear, *Numerical Initial Value Problems in Ordinary Differential Equations* (Prentice-Hall, Engelwood Cliffs, NJ, 1971).
[29] K. Kassner, C. Misbah, H. Müller-Krumbhaar, and A. Valance (unpublished).
[30] B. A. Malomed and M. I. Tribelsky, Physica **D14**, 67 (1984); M. R. E. Proctor and C. A. Jones, J. Fluid Mech. **188**, 301 (1988); H. Levine, W. J. Rappel, and H. Riecke, Phys. Rev. A **43**, 1122 (1991).
[31] S. Fauve, S. Douady, and O. Thual, Phys. Rev. Lett. **65**, 385 (1990).
[32] B. Caroli, C. Caroli, and S. Fauve, J. Phys. (France) I **2**, 281 (1992).

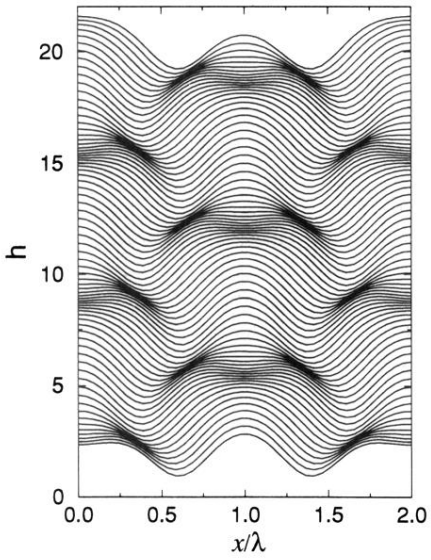

FIG. 14. Spatiotemporal portrait of the VB mode ($\alpha=0.1$, $q=0.64$).

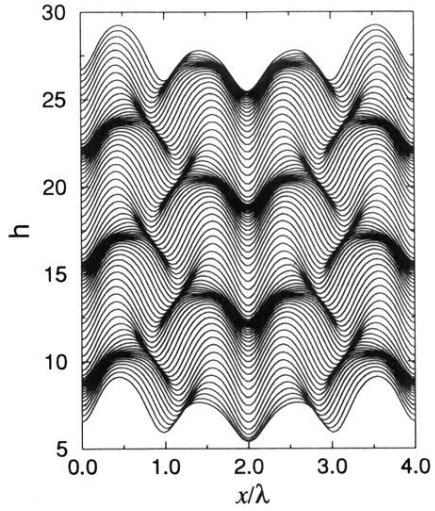

FIG. 15. Spatiotemporal portrait of the IVB mode ($\alpha=0.05$, $q=0.68$, $Q/q\simeq 0.3$).

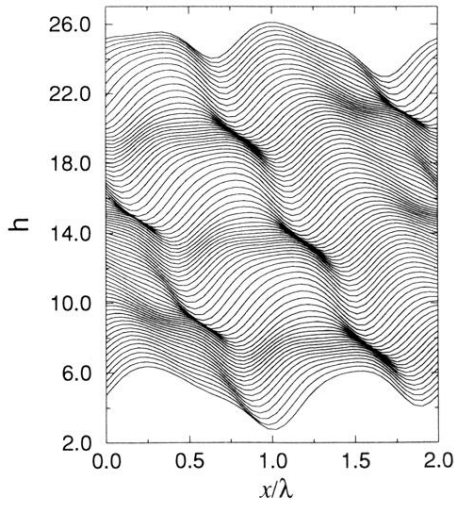

FIG. 20. Spatiotemporal portrait showing a mixture of a VB and a BP mode ($\alpha=0.048$, $q=0.53$).

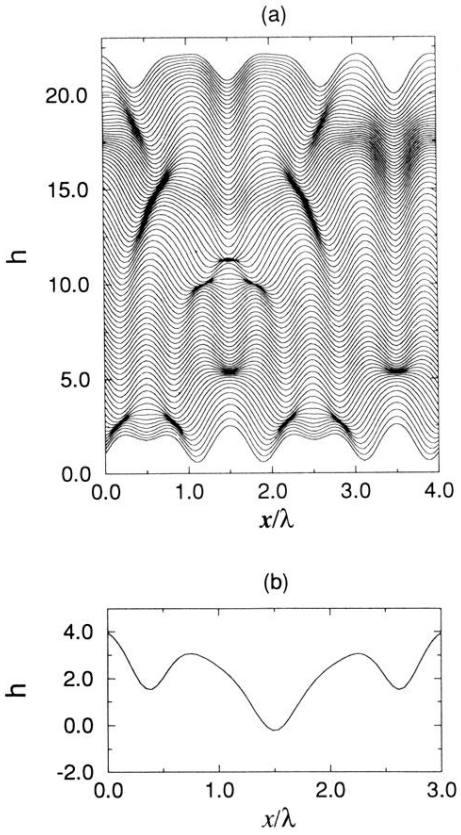

FIG. 21. Dynamics showing the creation of pairs of anomalous cells and their destruction and so on (a). In (b) we have plotted the anomalous cells.